Molecular Dynamics Simulations of Charged Dendrimers: Low-to-Intermediate Half-Generation PAMAMs

ARTICLE *in* THE JOURNAL OF PHYSICAL CHEMISTRY B · SEPTEMBER 2007

Impact Factor: 3.3 · DOI: 10.1021/jp072211x

3 AUTHORS, INCLUDING:

Jose Nuno A Canongia Lopes
Technical University of Lisbon
179 PUBLICATIONS **8,341** CITATIONS
SEE PROFILE

Sílvia Brito Costa
Technical University of Lisbon
181 PUBLICATIONS **2,807** CITATIONS
SEE PROFILE

Molecular Dynamics Simulations of Charged Dendrimers: Low-to-Intermediate Half-Generation PAMAMs

Pedro M. R. Paulo,* José N. Canongia Lopes, and Sílvia M. B. Costa

Centro de Química Estrutural—Complexo 1, Instituto Superior Técnico, Av. Rovisco Pais, 1049-001 Lisboa, Portugal

Received: March 20, 2007; In Final Form: June 8, 2007

We have performed atomistic molecular dynamics simulations of PAMAM dendrimers of generations 0.5, 1.5, 2.5, 3.5, and 4.5. The simulated systems comprise the charged dendrimer and its counterions embedded in a dielectric continuum (i.e., without explicit solvent). Structural properties of these dendrimers, like the radius of gyration, the principal moments of inertia, and the segment density profiles, were evaluated from the simulations. The average radius of gyration obtained for the intermediate half-generations 2.5, 3.5, and 4.5 follows the same scaling law that was previously inferred from simulations of full-generation PAMAMs, $R_g \approx M^{1/3}$, and is characteristic of space-filling objects. The low half-generations 0.5 and 1.5 deviate, however, to greater R_g values. The shape of the smaller dendrimers is approximately that of a prolate ellipsoid, which becomes more spherical for higher generations. The segment density profiles show features identical to those obtained in other simulations of flexible-chain dendrimers, like dendron-backfolding. Two slightly different configurations, in terms of size and shape, were identified for generation 2.5. The radial distributions of counterions extracted from the simulations compare well with the solutions of Poisson−Boltzmann cell model, and the dendrimer's effective charge was estimated using the Bjerrum criterion. The influence of electrostatic interactions in the dendrimer's conformation due to repulsion between the charged end-groups and its relation to counterion effects is discussed for the several generations simulated. The form factors calculated from the simulations are compared with the model of a homogeneous ellipsoid of revolution. The overall results are in agreement with the previously established morphological transition of PAMAM dendrimers toward a more spherical and compact conformation above generations 3 or 4.

1. Introduction

Dendrimers differentiate from other hyperbranched polymers due to their regular topology in terms of chemical structure. These macromolecules were first synthesized in the early 1980s with the development of synthetic strategies involving successive protection−deprotection steps (cascade synthesis).[1,2] Although an aesthetic appeal must have been one of the original motivations to grow such chemical structures, several applications for dendrimers have been sought and proposed in the literature.[3−5] The set of potential applications encompass a variety of areas, namely biology (as mimetic systems of enzymes or redox proteins),[6−10] medicine (in drug delivery, gene therapy, and biochemical sensors),[3,4] optoelectronics (for transduction of signals or light-harvesting devices),[11−14] and nanoscience (as building units in self-assembled systems or functionalized with groups for molecular recognition and signaling).[3,4,15−17]

Poly(amido)amine or PAMAM dendrimers are among the most studied families of dendrimers, which is certainly related to their early appearance in the field and also to their commercial availability. These organic dendrimers contain tertiary amines as branching points, i.e., the respective branching multiplicity is 2. The core multiplicity varies; the original PAMAM dendrimers were synthesized from an amine core and thus had a 3-fold multiplicity,[1,6] whereas recently, ethylenediamine−core PAMAMs became more common and these have a 4-fold multiplicity[18] (Figure 1). The typical end-groups are primary amines or carboxylate functions depending on if these are full- or half-generation PAMAMs. In the latter case, the dendrimer synthesis is interrupted in the first of a two-step mechanism for growing the next layer of monomers (usually termed generations).[2] This results in a terminal layer having spacer units

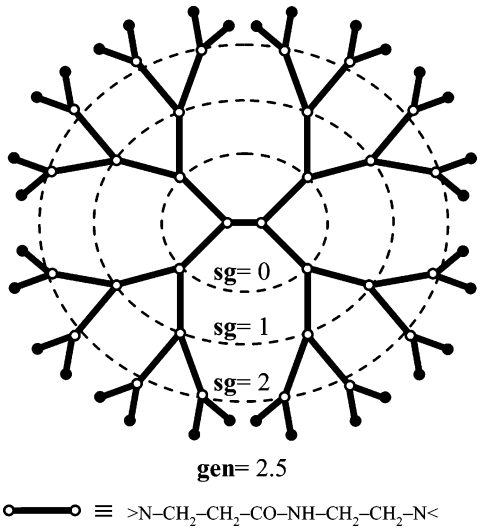

Figure 1. Topology of simulated PAMAM dendrimer of generation 2.5: open and closed circles represent the branching points and terminal groups, respectively; the dashed lines indicate the monomer layers that constitute each of the subgenerations (sg).

* Corresponding author. E-mail: pedro.m.paulo@ist.utl.pt.

10.1021/jp072211x CCC: $37.00
Published on Web 08/18/2007

that are roughly half the length of the monomers in the lower generations (or subgenerations).

The polyelectrolyte character of PAMAMs derives from the acid−base functional groups that constitute the branching and terminal points. Full-generation PAMAMs are neutral at high pH and become positively charged around pH 7 due to protonation of the terminal primary amines. At lower pH conditions, the dendrimer's charge is further increased by protonation of the tertiary amines in the branching points. By opposition, half-generation PAMAMs can bear negative charges from dissociation of the terminal carboxylate groups. Furthermore, taking into consideration the typical pK_a values of carboxylic acid functions and of the dendrimer's tertiary amines,[19] it is conceivable that, within a restrict interval of pH, the half-generations became zwitterionic (i.e., with the end-groups negatively charged and some branching points positively charged).

Full-generation PAMAM dendrimers have been investigated more extensively and properties such as the size, shape or conformation, spatial distribution of terminal groups, chain dynamics, acid−base behavior, and counterion or metal binding, among others, have been evaluated from both experimental[1,6,20−33] and theoretical[34−40] or computational[41−48] standpoints. The effect of solvent quality or pH and ionic strength in the dendrimer size and conformation has received particular attention.[38,44,46,49−55] Although half-generation PAMAMs are not so well characterized in the literature, several studies have been reported in some applied areas such as interaction with drugs and drug delivery,[56−66] crystallization processes,[67−75] and environmental and analytical chemistry.[76−78] Other studies include the interaction of half-generation PAMAMs with surfactants,[79−82] polymers,[83,84] and fluorescent probes.[85−89]

Simulations with coarse-grained models certainly represent a very important and judicious way to characterize the unique features of flexible-chain dendrimers, like dendron-backfolding or counterion effects,[42−45,55] but this simplified approach could overlook specific physical or chemical interactions in the simulated systems. In this sense, atomistic simulations, in the framework of classical molecular dynamics, offer some improvement at the expense of greater computational effort. The present study employs atomistic molecular dynamics simulations to evaluate the structural properties of half-generation PAMAM dendrimers, whereas up to now, the atomistic simulation studies known from the literature have addressed only the full generations.[41,46,48,53,54] Besides, the optimized potential for liquid simulations (OPLS) force field[90−98] used here is applied for the first time to the simulation of PAMAM dendrimers. The OPLS force field can be regarded as a development of the AMBER force field, and the latter was optimized for the simulation of nucleic acids and proteins.[99,100] PAMAM dendrimers have several functional groups in common with proteins (e.g., amide, amine, and carboxylate groups), which makes OPLS an appropriate force field to model this type of dendrimers. To the best of our knowledge, this is the first account on simulation of half-generation PAMAMs and also on the application of an OPLS-based force field to the simulation of dendrimers.

In our simulations, it was assumed that the dendrimer's carboxylate groups are dissociated and therefore each contributes with an elementary charge unit for its structural charge (other functional groups are assumed to be noncharged). This implies that counterions must be introduced to maintain the electroneutrality of the simulated systems. The effect of counterions in the simulation of charged dendrimers were addressed in two recently published independent studies; Maiti et al.[53,54] performed atomistic simulations of full-generation PAMAMs with explicit solvent and counterions, whereas Gurtovenko et al.[55] used a "bead-and-spring" model to evaluate the effects of varying the strength of electrostatic interactions in salt-free dendrimer solutions. Our simulations can be considered at an intermediate level of sophistication because we used an atomistic model without explicit solvent. The dendrimer and the counterions are assumed to be embedded in a dielectric continuum with constant permittivity. Explicit solvent was not introduced in our simulations to make possible the use of simulation boxes large enough to correspond to the low dendrimer concentrations employed in our experimental studies of systems involving PAMAM dendrimers.[89,101]

TABLE 1: Information about the Chemical Structure of Simulated PAMAM Dendrimers: Molecular Weight (M), Number of Atoms (N_{atoms}), and Number of Terminal Carboxylate Groups (N_{term}).

generation	M/Da	N_{atoms}	N_{term}
0.5	1269.0	148	8
1.5	2934.6	356	16
2.5	6265.7	772	32
3.5	12927.8	1604	64
4.5	26252.1	3268	128

The present paper is organized in the following manner: the application of the OPLS force field to PAMAM dendrimers is outlined in Section 2, all calculations and results based on the simulation data and the corresponding discussion are presented in Section 3, and finally, the concluding remarks are given in Section 4.

2. Model and Methods

The molecular dynamics simulations were performed with the commercially available program DL_POLY.[102] Typical values were assumed for the bond lengths and angles to construct the *z*-matrix of the initial configuration of the simulated dendrimers (see Supporting Information). The torsional angles were directly adjusted to avoid conformations with complex chain entanglements. The initial configurations thus obtained are relatively extended and were relaxed by the equilibration procedure described later in this section. The topology of the simulated dendrimers is exemplified in Figure 1 for generation 2.5 (other generations can be derived from self-similarity). Some data concerning the chemical structure of the simulated half-generation PAMAMs are given in Table 1. The number of terminal groups (N_{term}) corresponds also to the number of sodium counterions that were added to each simulation box. A cubic box with a side length of 321.4 Å (a volume of 33200 nm^3) was employed in all simulations except when stated otherwise. One dendrimer molecule contained in such a volume is equivalent to a dendrimer concentration of 0.05 mM. Periodic boundary conditions and minimum image convention were assumed in the calculation of particle interactions.

As previously mentioned, we used the OPLS force field in our simulations. The parameters for the potential functions of the monomer segments were adapted from the values proposed for *N*-methylacetamide.[95] For the branching points and terminal groups, the same parameters were taken from amino acids with tertiary amines and carboxylate functions (a comprehensive list of force field parameters is provided in the Supporting Information).[94,96] Bond constraints were assumed for the bonds involving H atoms by application of the SHAKE algorithm. This allowed using a time step of 1 fs in the simulations because the high-frequency motions of bonds involving H atoms were constrained to the corresponding equilibrium distances.

All simulations were performed at 298 K. The temperature was adjusted with the Nosé−Hoover thermostat assuming a thermal bath coupling constant of 1 ps.[103] The pressure of 1 bar was imposed by application of the Hoover barostat with a coupling constant of 4 ps. Because explicit solvent was not considered in our simulations, a relative permittivity of 78.4 (equivalent to water at 298 K) was assumed for the calculation of electrostatic interactions. These were computed using the Ewald method with the corresponding α parameter and the top limits of the *l*, *m*, and *n* factors being automatically determined by the routines programmed in DL_POLY and with a standard precision of 10^{-6}.[102] A cutoff distance of 50 Å was defined for the calculation of the long-range potential terms. This allowed us to account for all the interactions between atoms not directly bonded within the same dendrimer. A Verlet list of neighboring particles was also defined for a distance of 60 Å beyond the cutoff distance. The van der Waals interactions were handled by Lennard-Jones potential terms, according to OPLS parametrization, and nonbonded interactions of order higher than two were not explicitly accounted for.

It must be stressed at this point that the choice of a constant permittivity value for the simulations was analyzed at a preliminary stage of our work. In this sense, we have also used distance-dependent dielectric constants for the simulation of full-generation (2.0 and 4.0) PAMAM dendrimers (cf. beginning of Section 3A). The results obtained did not show striking differences between the simulations with constant and distance-dependent dielectric constants, both in terms of the average radius of gyration and the segment density profiles or the respective form factors. However, preliminary simulations of generation 2.5 considering a distance-dependent dielectric constant yielded counterion radial distributions that did not compare well with the respective solution of the Poisson−Boltzmann equation. This was not the case for simulations considering a constant permittivity value (that of bulk water). Therefore, it was assumed that the choice of a constant permittivity ($\epsilon = 78.4$) gives a better description of the interactions of the charged terminal groups of the dendrimer with its counterions. Although this may seem a poor approximation for the inner regions of the dendrimer, the full-generation results show that (probably due to topological reasons associated with the extremely ramified nature of the dendrimers and the lack of secondary or tertiary protein-like structures) the use of a constant or distance-dependent dielectric constant in those regions is not a crucial factor.

Preparation of the starting configurations for the simulations comprised two steps. First, the dendrimer initial configuration was relaxed in the absence of counterions during 10 ps with an initial 2 ps period of equilibration. Then the counterions were added to the simulation box with a radial distribution sampled from the ionic profile estimated from the Poisson−Boltzmann equation (see Section 3C) using a Monte Carlo simulation routine. The polar and azimuthal coordinates of the counterions were uniformly distributed over the range of possible values. The system constituted by the dendrimer and its counterions was simulated during 120 ps with an initial equilibration period of 20 ps to allow for further relaxation. The end configuration of this simulation run was assumed as the starting configuration for the actual simulation (this procedure was repeated for each dendrimer system). The simulation runs were initiated by another 20 ps equilibration period and were then extended by: 400 ps for generations 0.5 and 1.5, 300 ps for generation 2.5, and 200 ps for generations 3.5 and 4.5. Computations were mostly performed in a single Pentium IV 3.0 GHz processor.

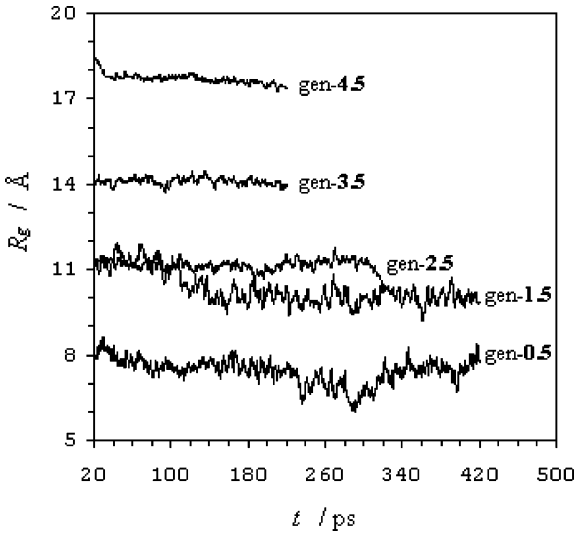

Figure 2. Time evolution of the dendrimer radius of gyration during the simulation runs of different PAMAM dendrimer generations.

3. Results and Discussion

A. Size and Shape of Dendrimers. The size of the simulated dendrimers was evaluated from the mean-square radius of gyration, which is defined as

$$R_g^2 = \frac{1}{M}\sum_{i=1}^{N} m_i |\mathbf{r}_i - \mathbf{R}_0|^2 \qquad (1)$$

for a body constituted by *N* discrete particles where *M* is the total mass, m_i and $\mathbf{r}_i$ are, respectively, the mass and position of the *i*th particle, and $\mathbf{R}_0$ is the center-of-mass of the body. Figure 2 depicts the evolution of R_g (every 0.1 ps) throughout the simulation runs for generations 0.5 up to 4.5 after the initial equilibration procedure. During the equilibration, the R_g trajectory exhibits a monotonic decrease (which accompanies relaxation from the initial over-tensioned configuration to an equilibrated one) and then it stabilizes, apart from random oscillations due to conformational flexibility of the dendrimer structure. These oscillations are more pronounced for the lower generations that are stereochemically less restrained. In general, the simulation results presented in this section were averaged over the last 100 ps time interval of the trajectories shown in Figure 2 to ensure that these correspond to equilibrium quantities.

In Figure 3A, the average radius of gyration ($R_g \equiv \langle R_g^2 \rangle^{1/2}$) for the simulated dendrimers is compared to the values obtained by other authors for atomistic simulations of full-generation PAMAMs using different force fields (CVFF[46] and Dreiding[48,53]) and different simulation conditions (distance-dependent dielectric "constant"[46] and gas-phase[48] or explicit solvent and counterions[53]). We have also simulated full-generation PAMAM dendrimers using the OPLS force field and a distance-dependent dielectric "constant" to validate our model of PAMAM dendrimers by direct comparison with the literature results. The R_g values calculated from our simulations of generations 2.0 and 4.0 (open circles in Figure 3A) compare satisfactorily with the R_g values of other simulations of noncharged (neutral) dendrimers in the absence of solvent (open triangles and squares in the same figure). From early nonatomistic computational models of flexible-chain dendrimers, it was inferred that these obey a scaling law of the type $R_g \approx M^{1/d_f}$, where *M* is the molecular weight and d_f is the fractal dimension of the object. With the exception of the kinetic growth model

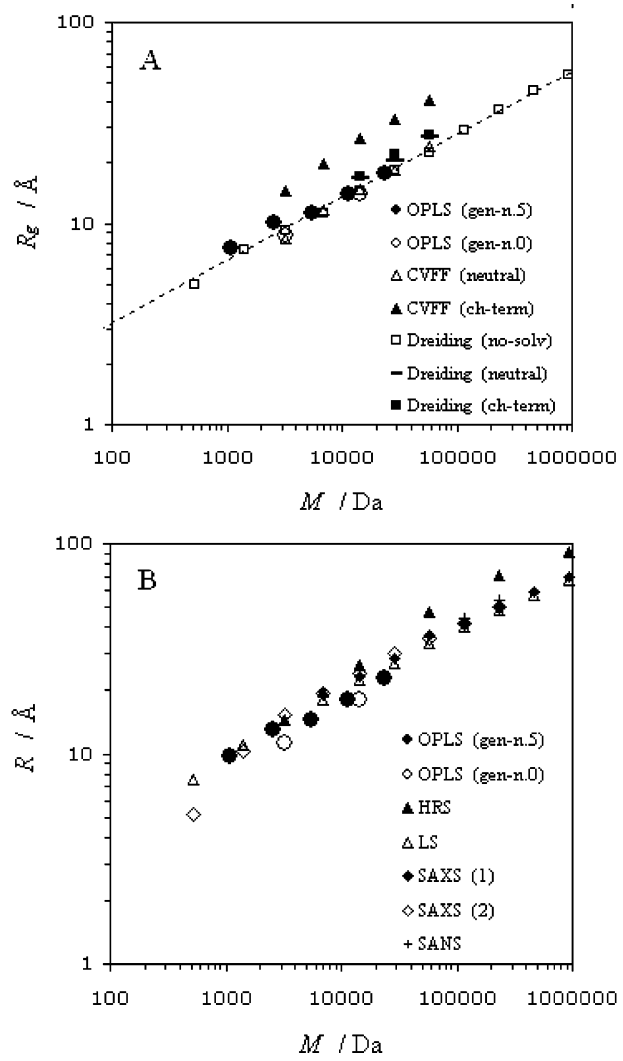

Figure 3. Average radii values calculated by simulation of half-generation PAMAM dendrimers (closed circles) and of full-generations 2.0 and 4.0 (open circles). (A) Comparison with the radius of gyration (R_g) from atomistic simulations from the literature: the data labeled "CVFF" were taken from ref 46 and the data labeled "Dreiding" were taken from refs 48 and 53. (B) Comparison with experimental hydrodynamic radius (R) from the literature: the data labeled "HRS" were taken from ref 20, the data labeled "LS" were taken from ref 1, the data labeled "SAXS(1)" were taken from ref 22, the data labeled "SAXS(2)" were taken from ref 24, and the data labeled "SANS" were taken from ref 50.

of Lescanec and Muthukumar[42] and the pioneer theoretical model of de Gennes and Hervet,[34] all the subsequent computational and theoretical studies agree that the power dependence on M is about 0.3, which gives a fractal dimension of 3 and thus lead to the conclusion that dendrimers are space-filling or compact objects (in opposition to what is suggested by the fractal topology of their chemical connectivity). This feature is illustrated in Figure 3A by the dashed line, which represents a power law fitted to the R_g values of generations 2.5, 3.5, and 4.5 from our simulations (closed circles in Figure 3A). The value retrieved for the M exponent is 0.31, in agreement with the preceding remarks. Furthermore, the R_g values of (the intermediate) half-generations fall in the same trend as the values for the simulations of full-generation PAMAMs in the absence of solvent. The same is, however, not valid for (the low) generations 0.5 and 1.5 that have R_g values slightly above the trend defined by the other simulation results.

The conformation of flexible-chain dendrimers can be rationalized in terms of the interplay between opposing contributions: excluded-volume interactions between monomers promoting extension of branches and the conformational entropy penalty associated with it. In the case of charged dendrimers, the intramolecular repulsion between charged groups due to electrostatic interactions or osmotic pressure effects due to counterion condensation must also be considered. The counterion concentration increases exponentially with dendrimer generation because it is proportional to the number of terminal groups $-N_{term} = 4 \times (2^{g+1} - 1)$, where g is the dendrimer generation (see Table 1).[104] Therefore, in the absence of added salt, the screening effect of the electrostatic interactions by the dendrimer's counterions must be more significant for higher generations. The Debye screening length κ^{-1} can be used to assess the relative importance of electrostatic interactions,

$$\kappa^2 = 4\pi l_B \sum_i c_i z_i^2 \tag{2}$$

Here c_i and z_i are the concentration and charge of the ith ion in solution and l_B is the Bjerrum length, which is defined as

$$l_B = \frac{e^2}{4\pi\epsilon\epsilon_0 k_B T} \tag{3}$$

where ϵ is the relative permittivity of the solvent and the other symbols have the usual meaning. For the conditions defined in our simulations, κ^{-1} assumes the values of 215, 152, 108, 76, and 54 Å when going from generation 0.5 to 4.5, showing that electrostatic interactions, like repulsion between charged terminal groups, are more important for lower generations. This partially explains the relatively more extended conformations of generations 0.5 and 1.5. Other factors, such as counterion condensation and molecular packing in higher generations, cannot be dismissed and will be discussed in the following sections.

In explicit-solvent simulations, Maiti et al.[53] have observed a swelling effect in PAMAM dendrimers of generations 4.0 to 6.0, which translates into an increase of 10−15% in the radius of gyration (gray squares in Figure 3A). Upon protonation of the terminal groups, these authors observed no significant changes in the dendrimer's radius of gyration (closed squares in Figure 3A). This is due to limitations in the size of the simulated systems (because both explicit solvent and counterions are considered in their simulations) that imply high counterion concentrations. The screening effects (corresponding to κ^{-1} values in the range 3−4 Å) preclude any measurable changes in the dendrimer conformation due to electrostatic repulsion of the charged terminal groups. On the other hand, Lee et al.[46] obtain an increase of 70−80% in the radius of gyration of generations 2.0 to 6.0 upon protonation of the terminal groups (closed triangles in Figure 3A). This pronounced increase is probably overestimated due to the absence of counterions in their simulations. Thus, the variations observed for the size of charged dendrimers in that work could be perceived as top limits for the variations in real systems. It is not possible to directly compare our results for charged PAMAM dendrimers with those from the literature because the simulation conditions are significantly different.

In Figure 3B, the average hydrodynamic radius for the simulated dendrimers (estimated from an approximation to spherical objects $R = \sqrt{5/3}R_g$) are compared to experimental values obtained for full-generation PAMAMs (half-generation PAMAMs are not so well-characterized and systematic studies

of their structural properties are lacking). In general, the experimental values are slightly higher, which can be explained by solvent swelling effects. Comparison with the dimensions estimated for PAMAM dendrimers from simulations with explicit solvent seems to indicate that this is the case.[53] Despite some scattering in the experimental data, the overall trend seems to follow a scaling law similar to that found from simulations and theoretical models. It would be interesting to experimentally assess in a systematic way the influence of solvent quality, pH, and ionic strength in the dendrimer dimensions and to evaluate if part of the scattering in the experimental data is related to different medium conditions. Some of these issues were already addressed by SANS studies for a limited number of dendrimer generations and small (about 10%) or inexistent effects were observed.[50,51]

It is common knowledge that flexible-chain dendrimers, although being chemically regular structures, do not assume regular shapes (Figure 4). To quantitatively evaluate the deviation of the dendrimers' shape from spherical symmetry, the principal moments of inertia were calculated from diagonalization of the inertia tensor,

$$\mathbf{I} = \sum_{i=1}^{N} m_i[(\mathbf{r}_i \cdot \mathbf{r}_i)\mathbf{1}_3 - (\mathbf{r}_i \mathbf{r}_i^{\mathrm{T}})] \tag{4}$$

where $\mathbf{r}_i$ is the position of ith atom relative to the center-of-mass of the molecule and $\mathbf{1}_3$ is the unitary matrix of dimension 3. The eigenvalues of $\mathbf{I}$ computed from the simulations can be ordered in the following manner: $I_x < I_y \cong I_z$, i.e., the simulated dendrimers are approximately prolate ellipsoids (Table 2). Our results for the full-generations 2.0 and 4.0 (not shown here) give $I_{y,z}/I_x$ ratios lower than those obtained by Maiti et al.,[48] which means that we observe dendrimer structures that are more spherical. The average $I_{y,z}/I_x$ ratios calculated for the half-generation dendrimers are represented in Figure 5. Lower generations are more eccentric, in accordance with previous results on full-generation PAMAMs.[105] With increasing dendrimer generation the $I_{y,z}/I_x$ ratios converge toward unit, reflecting more spherical conformations. This is accompanied by a decrease in the amplitude of the $I_{y,z}/I_x$ oscillations along the simulation trajectory (measured by the error bars in Figure 5). Indeed, for all dendrimer generations covered in our work, only generation 4.5 has a quasispherical distribution of mass, although such a fact is not obvious in the simulation snapshot presented Figure 4E. The parameter of asphericity defined by Rudnick and Gaspari[106] was also employed to ascertain deviations from spherical shape,

$$\delta = 1 - 3\frac{\langle I_2 \rangle}{\langle I_1^{\,2} \rangle} \tag{5}$$

where I_1 and I_2 refer to the first and second invariants of the inertia tensor

$$I_1 = I_x + I_y + I_z \tag{6}$$

$$I_2 = I_x I_y + I_y I_z + I_x I_z \tag{7}$$

The δ values obtained for the simulated dendrimers are also plotted in Figure 5. The similarity with the trends observed for the $I_{y,z}/I_x$ ratios is evident. Our results for the half-generations are in agreement with previous computational studies of full-generation PAMAMs which identify a transition toward more spherical dendrimer shapes above generations 3 or 4.

B. Segment Density Profiles. The segment density profiles provide information about the internal structure of the simulated dendrimers in terms of the radial distribution of mass. The density profiles are calculated by summing the mass contribution of each atom within a spherical shell of radius r and thickness Δr

$$\rho(n\Delta r < r < (n+1)\Delta r) = \frac{1}{V_{n,\Delta r}} \sum_{i=1}^{N} m_i \times H(r_i - n\Delta r)H((n+1)\Delta r - r_i) \qquad n = 0,1,... \tag{8}$$

where $V_{n,\Delta r}$ is the volume of the spherical shell, m_i and r_i are, respectively, the mass of the ith atom and its distance to the dendrimer's center-of-mass and $H(x)$ is the Heavyside function.[107] In this work, a shell thickness of $\Delta r = 1$ Å was used in the data treatment and the final density profiles were averaged from 1000 configurations equally spread over the last 100 ps of simulation. The segment density profiles were computed for the whole dendrimer and also for each of the generations into which it can be decomposed. For instance, a 2.5 generation dendrimer can be regarded as a 0.0 generation core surrounded by succeeding 1.0, 2.0, and 2.5 generation layers (see again Figure 1). These generation layers are hereafter referred to as subgenerations (sg) to distinguish them from the last generation that usually defines the dendrimer as a whole.

The overall density profiles for the lower generations simulated (Figure 6A,B) exhibit a sharp maximum near the dendrimer's center-of-mass and then decrease almost monotonically toward its periphery. In contrast, the profiles of generations 2.5 and 3.5 show minima at the center-of-mass that evolve to a region of roughly constant density and finally decay smoothly (Figure 6C,D). Maiti et al.[48] also observed a change from a maximum of density near the center-of-mass to a minimum with increasing generation in their simulations of PAMAM dendrimers. This trend is, however, not entirely confirmed by our results because the density distribution of generation 4.5 shows a maximum at $r = 0$ (Figure 6E). Several coarse-grained computational models and theoretical studies of flexible-chain dendrimers predict a radial density profile with a sharp maximum near the center-of-mass followed by a local minimum followed by a region of approximately constant density (the plateau region) that eventually decays.[38,43,44] This qualitative description fits quite well the density profile obtained for generation 4.5.

The overall density profiles for all simulated half-generations are superimposed in Figure 6F. The tail region spreads over greater distances as the dendrimer generation increases and it decays in a similar smooth fashion. The range of generations covered in this work is not comprehensive enough to allow us to observe an increase of the density at the plateau region or an increase in the length of the tail region with increasing generation in analogy with the results of Maiti et al. for full-generations, in which case PAMAMs up to generation 11 were simulated.[48] The average density of the simulated dendrimers is ca. 0.5 g/cm^3 for generations 0.5 and 1.5, and it increases to about 0.8−0.9 g/cm^3 for generations 2.5, 3.5, and 4.5. The latter range of densities is close to the value of 0.78 g/cm^3 estimated by Nisato et al. for PAMAM generation 8 in aqueous solution using SANS technique.[51]

The density profiles of the subgenerations extend out radially as the dendrimer generation progresses from 0.5 to 4.5. However, starting from generation 2.5, it is possible to verify that the density profiles of the larger subgenerations, in particular the terminal subgeneration, also extend to regions close to the

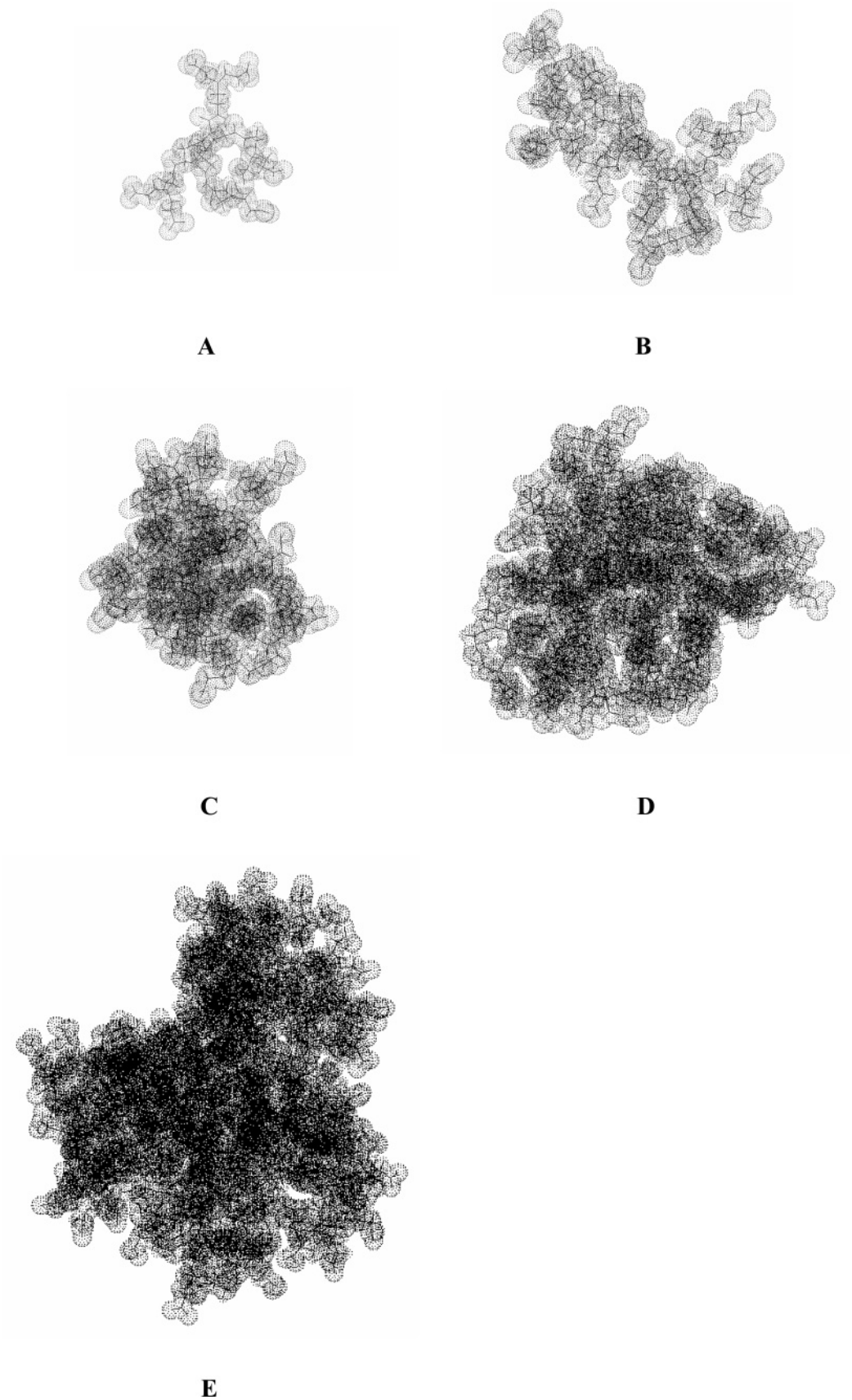

Figure 4. Snapshots of dendrimer configurations sampled from the simulation runs: (A) generation 0.5, (B) generation 1.5, (C) generation 2.5, (D) generation 3.5, (E) generation 4.5.

dendrimer's center-of-mass. This means that the terminal groups are not confined to the external regions of the dendrimer but are distributed throughout its structure. This phenomenon is well-known from computational models of dendrimers and the term "dendron backfolding" was coined to describe it.[43,44] The spatial distribution of the larger subgenerations that partially

TABLE 2: Average Values of the Radius of Gyration (R_g), the Principal Moments of Inertia (I_x, I_y, I_z), and the Parameter of Asphericity δ Calculated for the Simulated PAMAM Dendrimers

generation	R_g [Å]	I_x [10^3 amu Å^2]	I_y [10^3 amu Å^2]	I_z [10^3 amu Å^2]	δ
0.5	7.5 ± 0.3	23 ± 3	42 ± 4	57 ± 5	0.06 ± 0.01
1.5	10.0 ± 0.2	67 ± 5	210 ± 15	241 ± 13	0.10 ± 0.01
2.5	11.2 ± 0.2	270 ± 7	471 ± 16	509 ± 12	0.047 ± 0.009
3.5	14.1 ± 0.1	944 ± 32	1609 ± 45	2001 ± 42	0.041 ± 0.003
4.5	17.6 ± 0.1	4079 ± 59	4857 ± 86	5492 ± 166	0.007 ± 0.002

occupy the dendrimer's internal volume, releases some of the tension resulting from steric congestion in the peripheral regions imposed by the exponential growth of the dendrimer structure with increasing generation (see again Figure 4). This occurs at the expense of an increase of the tension on the lower subgenerations that stretch out in order to accommodate the backfolded dendrons. This is usually referred to as a "pulling effect", and it is quantified by determining the distribution of distances between branching points connected by monomer segments or the distribution of angles between the vectors that connect these branching points.[48] Another interesting feature about the dendrimer's internal structure that was inferred from simulations is "dendron segregation", i.e., the different branches of a dendrimer are only slightly overlapped.[44]

C. Counterion Radial Distribution and Counterion Condensation. The radial distributions of counterions were computed from the simulation results in a similar way to the density profiles, i.e., by applying expression 8 to the counterion particles in the simulation box disregarding, however, the mass prefactor. These are plotted in Figure 7 in a cumulative form,

$$N_{ci}(r) = \int_0^r \rho_{ci}(s) 4\pi s^2 \, ds \tag{9}$$

where $\rho_{ci}(r)$ is the number density profile of counterions (for a spherical cell of radius L, it is verified that $N_{ci}(L)$ is equal to the total number of counterions). For comparison, the solutions of Poisson−Boltzmann (P−B) cell model were calculated for conditions similar to those of the simulations.[108,109] Within the framework of this model, the dendrimer is approximated to a charged sphere embedded in a dielectric continuum and the counterions are treated as non-self-interacting charged points. This simplifies Poisson−Boltzmann equation to,

$$\frac{1}{r^2}\frac{d}{dr}\left(r^2 \frac{d\phi}{dr}\right) = 4\pi l_B N_A \sum_i c_i Z_i \, e^{Z_i \phi} \tag{10}$$

where l_B is the Bjerrum length, Z_i is the valence of species i and c_i is a quantity related to its average concentration, C_i,

$$C_i = c_i \langle e^{Z_i \phi} \rangle = \frac{c_i}{L^3/3} \int_{R_D}^{L} e^{Z_i \phi} r^2 \, dr \tag{11}$$

The numerical solution of eq 10 (for the details see ref 89) yields the reduced potential function, $\phi = -e\,\psi/k_B T$, from which the ionic profiles can be derived by using

$$\rho_{ci}(r) = c_i \, e^{-Z_i \phi(r)} \tag{12}$$

in conjunction with eq 9, though changing the low limit of the integral expression to the hard-sphere radius.[110] This was approximated by the hydrodynamic radius estimated for the simulated dendrimers (Figure 3B). The counterion profiles calculated from P−B cell model (solid lines in Figure 7) compare very well with the counterion distributions extracted from the simulations.[111] This is coherent with the fact that both the simulation and P−B cell models assume the solvent as a dielectric continuum. Furthermore, because the simulation procedure accounts for ion−ion correlations, which are disregarded in the P−B cell model, the observed agreement indicates that such effects are not significant for the simulated conditions, thereby justifying the use of P−B cell model.

Simulation snapshots show a significant number of counterions residing inside or near the dendrimer's "surface". The localization of counterions in the vicinity of highly charged polyelectrolytes avoids the buildup of uncompensated electrostatic potential and is known as counterion condensation.[112,113] The following threshold has been proposed for the onset of charge localization upon spherical surfaces,[114]

$$\frac{R^2}{l_B Z_{str}} << \kappa^{-1} \tag{13}$$

where R and Z_{str} are, respectively, the radius and the structural or geometrical charge of the surface. This condition is verified for all simulated half-generation dendrimers, which implies that charge renormalization due to counterion condensation occurs in these macroion systems. To quantify this effect, the dendrimers' effective charge, Z_{eff}, was estimated from the P−B ionic profiles of Figure 7 using the Bjerrum criterion. According to this criterion, the counterions, which are within a radial distance up to the inflection point $\{Y, N_{ci}(Y)\}$ of its ionic profile, experience an electrostatic attraction that overcomes other

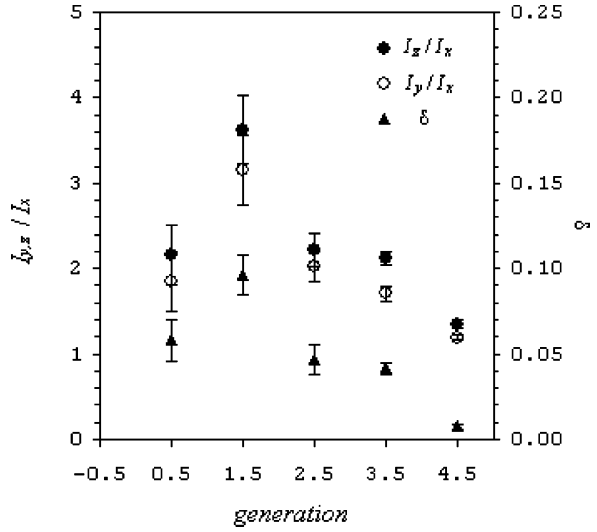

Figure 5. Ratios of the principal moments of inertia (I_z/I_x, full circles, and I_y/I_x, open circles) and values of the asphericity parameter (δ, closed triangles) as a function of dendrimer generation.

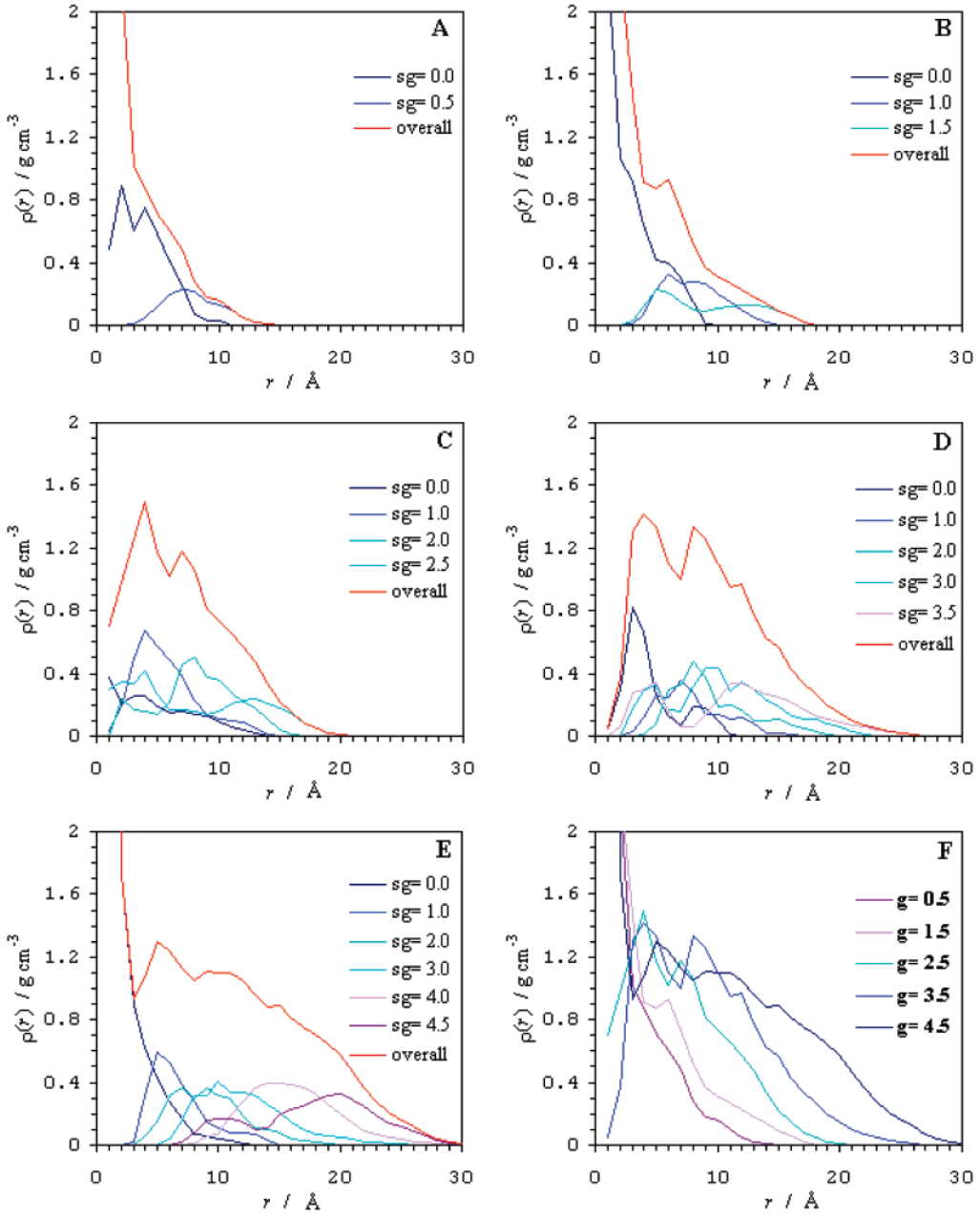

Figure 6. Segment density profiles (overall and corresponding subgenerations, sg) of the simulated half-generation PAMAM dendrimers: (A) generation 0.5, (B) generation 1.5, (C) generation 2.5, (D) generation 3.5, (E) generation 4.5, (F) superimposition of the overall segment density profiles for all simulated half-generations.

interactions and thus can be regarded as condensed counterions.[108] The effective charge of the macroion is then given by,

$$Z_{\text{eff}} = Z_{\text{str}} + Z_{\text{ci}}N_{\text{ci}}(\text{Y}) \qquad (14)$$

where Z_{ci} is the counterion valence. The values estimated for Z_{eff} of generations 0.5 up to 4.5 are: 7.7*e*, 12.9*e*, 16.4*e*, 19.8*e*, and 23.2*e*, respectively. This corresponds to a charge renormalization down to 96.5, 80.9, 51.1, 31.0, and 18.1% of the structural charge for those generations. Therefore, the electrostatic effects on dendrimer conformation should be more pronounced for the lower generations due to the higher relative effective charge. A similar conclusion was reached before based on the κ^{-1} values calculated for these systems (Section 3A).

Gurtovenko et al.[55] draw several interesting conclusions about the effects of counterions in salt-free solutions of charged dendrimers from their molecular dynamics simulations using a "bead-and-spring" model. Despite the similarities with the systems studied here, a direct comparison is not possible because these authors consider a different dendrimer topology[115] and also a different length of the simulation box,[116] which imply a counterion concentration different from our simulation conditions.

D. Configurations of Generation 2.5. Lower generations are less densely packed and thus show a greater conformational flexibility, as it can be perceived from the larger oscillations in the trajectories of R_g (Figure 2). Particular attention was dedicated to generation 2.5 in our simulations because experimental studies were also performed on systems involving this dendrimer generation by some of the authors (P.M.R.P. and S.M.B.C.).[89] From extended simulations, it was possible to identify two slightly different configurations for generation 2.5 based on the respective density profiles (Figure 8). As before,

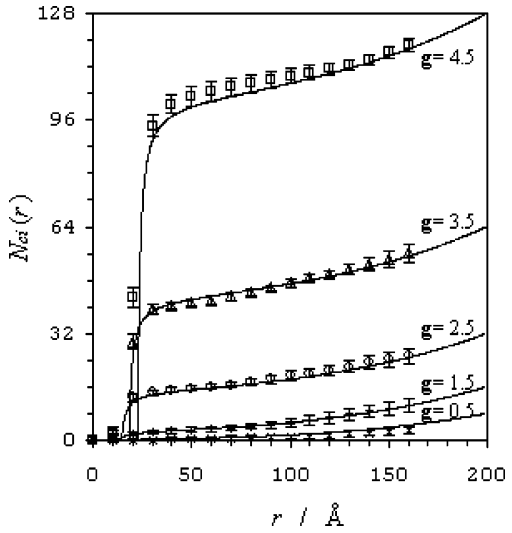

Figure 7. Radial distributions of counterions calculated for the simulated half-generation PAMAM dendrimers (symbols) and ionic profiles calculated from Poisson−Boltzmann cell model (full lines).

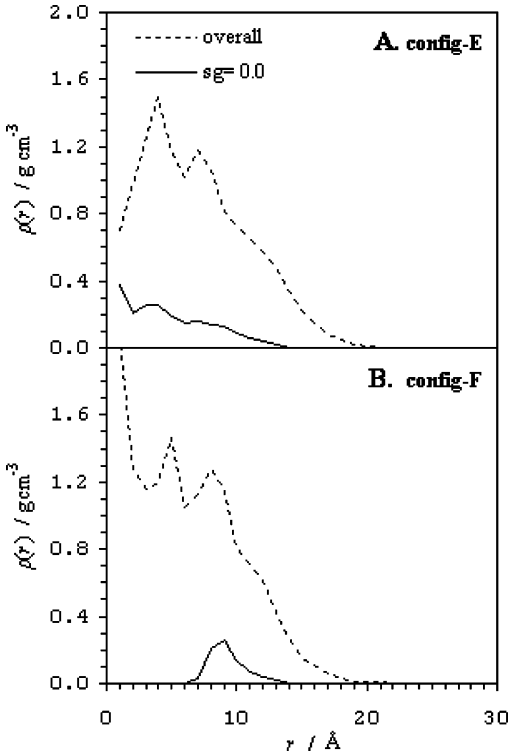

Figure 8. Segment density profiles of the configurations of type E (A) and type F (B) calculated from simulations of generation 2.5 dendrimers: overall density (dashed line) and subgeneration 0 density (full line).

the density profiles correspond to the average of 1000 configurations equally spread over a simulation period of 100 ps.

The density profiles of Figure 8A were already presented in Section 3B and are reproduced here to allow for direct comparison. In this case, the density profile of subgeneration 0 extends out from the center-of-mass, where its maximum is located. This corresponds to a more extended and ellipsoidal conformation with an average radius of gyration of $R_g = 11.2 \pm 0.2$ Å and an asphericity of $\delta = 0.047 \pm 0.009$. From here on, this configuration is labeled config-E. The density profiles of the other configuration (Figure 8B) show that the density of subgeneration 0 peaks at some distance away, ca. 9 Å, from the center-of-mass. For this to occur, the dendrimer branches should be preferably oriented over a hemisphere defined by a referential with its origin in the topological center of the dendrimer. This corresponds to a more compact and spherical conformation, as confirmed by the smaller values of $R_g = 10.6 \pm 0.1$ Å and $\delta = 0.032 \pm 0.004$. This configuration is labeled config-F.

These two configurations should be regarded as dynamic entities because other configurations with intermediate characteristics are obviously possible. Furthermore, in some simulations, it was possible to observe conversion between configurations with a density maximum for subgeneration 0 located near and away from the dendrimer's center-of-mass (config-E ↔ config-F). It is therefore assumed that the exploration of phase space over sufficiently long simulation periods should in principle return an ensemble of states with a realistic statistical distribution of conformations.[117] The use of Brownian dynamics methods would be interesting for this purpose because hydrodynamic effects can be introduced in the simulation without considering an explicit solvent. This would allow keeping the length of the simulation box at realistic values and to study the dynamics of conversion between conformations.

The observation of multiple configurations for flexible-chain dendrimers is not surprising, taking into account the many degrees of conformational freedom that these molecules possess. The topology of the potential energy surface of complex molecules can show complicated features, and it is possible that local minima with similar energies are located in different regions of configuration space.[118]

The effect of dendrimer concentration on its own conformation was studied for generation 2.5 using molecular dynamics simulations. This was accomplished by changing the length of the simulation box from 692.5 to 321.4 Å and 149.2 Å, which correspond to macroscopic dendrimer concentrations of 0.005, 0.05, and 0.5 mM, respectively.[119] Both configurations of type E and F were considered in this study. As previously done, the simulations were initiated with a 20 ps period of equilibration and were extended up to 320 ps. The data treatment was performed on configurations sampled from the last 100 ps of simulation.

By changing the length of the simulation box, the concentration of counterions and thus, the Debye screening length, also vary. This implies a variation in the magnitude of electrostatic interactions, which could affect the dendrimer's conformation due to repulsion forces between charged groups. The effect of concentration on the average radius of gyration and asphericity parameter of generation 2.5 is presented in Figure 9 (the larger Debye screening length, κ^{-1}, corresponds to the larger box length or lower concentration and so forth). The radius of gyration of config-E decreases with increasing concentration (closed circles in Figure 9). This corresponds qualitatively to the expected trend because the concomitant decrease in κ^{-1} is associated with greater screening of the electrostatic repulsion between the charged terminal groups. The asphericity parameter also decreases showing that the dendrimer assumes a more spherical shape (closed squares in Figure 9). The dendrimer's effective charge was estimated from P−B cell model with Bjerrum criterion and values of $Z_{eff} = 20.7e$, $16.4e$, and $12.2e$ were calculated for the concentrations of 0.005, 0.05, and 0.5 mM, respectively.[120] This is equivalent to a charge renormalization down to 65, 51, and 38% of the structural charge of generation 2.5 for the same concentrations, respectively. With increasing dendrimer concentration, its effective charge decreases and the electrostatic repulsion between charged groups becomes less important in comparison to the conformational

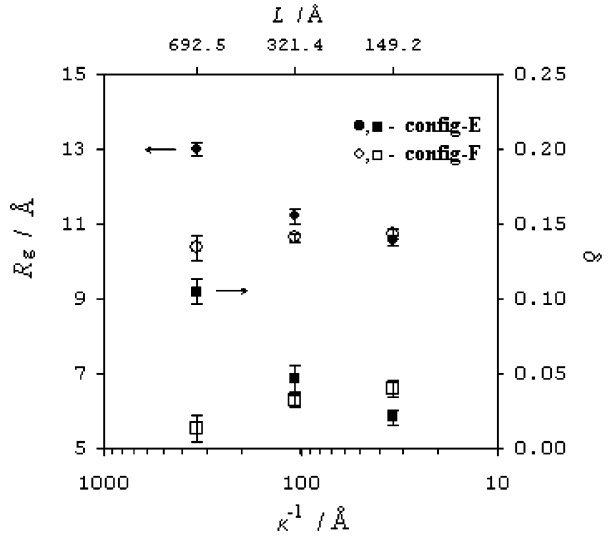

Figure 9. Average gyration radius (circles) and asphericity parameter δ (squares) as a function of the Debye screening length, κ^{-1} (or conversely, the simulation box length, L: upper axis) for configurations type E (closed symbols) and type F (open symbols) of generation 2.5.

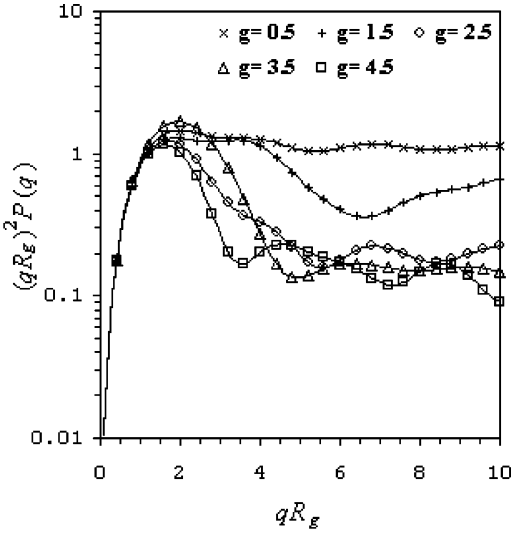

Figure 10. Kratky representation of the form factor $P(q)$ calculated for the half-generation PAMAM dendrimers simulated in this work: generation 0.5, crosses; 1.5, plusses; 2.5, circles; 3.5, triangles; and 4.5, squares.

entropy loss associated with extension of its branches, so the dendrimer assumes a more compact and spherical conformation. However, the same is not valid for the configuration of type F because negligible effects on the dendrimer's radius of gyration were observed upon variation of the concentration (open circles in Figure 9). We speculate that, in this case, the already compact conformation of the dendrimer makes it difficult to detect any appreciable effects from variations in the screening of electrostatic interactions.

E. Form Factors. The structure of PAMAM dendrimers in solution has been the subject of several studies reported in the literature using SANS and SAXS techniques.[21−24,49−51] The experimental quantity assessed is the scattering intensity $I(q)$, which can be expressed as,

$$I(q) \approx P(q)S(q) \tag{15}$$

where $P(q)$ is the form factor or the single-particle scattering funtion and $S(q)$ is the structure factor or the interparticle scattering function. The form factor $P(q)$ is the polar and azimuthal average of the Fourier transform of the single-particle density distribution, and it can be computed from simulation results using,[121]

$$P(q) = \frac{1}{4\pi N^2}\int_0^{2\pi}\int_0^{\pi} \left|\sum_{k=1}^{N} \exp(i\mathbf{q}\cdot\mathbf{r}_k)\right|^2 \sin\theta \, d\theta \, d\phi \tag{16}$$

where $\mathbf{q}$ is the scattering vector,[122]

$$\mathbf{q} = q\sin\theta\cos\phi\hat{e}_x + q\sin\theta\sin\phi\hat{e}_y + q\cos\theta\hat{e}_z \tag{17}$$

This was done by Maiti et al.[48] for their simulations of full-generation PAMAMs, and the calculated $P(q)$ functions compare well with the experimental SAXS scattering curves of Prosa et al.[22] Our results for generations 2.0 and 4.0 gave $P(q)$ curves (not shown here) that are identical to those obtained by Maiti et al. despite the small differences in size and shape of the simulated dendrimers as referred to in previous sections.

The form factors calculated for the half-generation PAMAM dendrimers simulated in this work are plotted in Figure 10 according to the Kratky representation. It is more intuitive to discuss form factors in the context of an appropriate model for the scattering objects, and several models have been proposed for flexible chain dendrimers: soft-sphere or star-like polymer, fuzzy edge sphere, rough sphere, hard-sphere with polydispersivity, ellipsoid of revolution, etc.[21,22,24] We restrain our discussion to the simple geometrical models of a homogeneous or hard sphere and of an ellipsoid of revolution. In the former case, the form factor can be expressed as $P(q) = F^2(q,R)$ with,[123]

$$F(q,R) = \frac{3[\sin(qR) - qR\cos(qR)]}{(qR)^3} \tag{18}$$

For an ellipsoid of revolution with semiaxes of length R, R, and ϵR, it applies

$$P(q) = \int_0^{\pi/2} F^2[q,r(R,\epsilon,\alpha)] \sin\alpha \, d\alpha \tag{19}$$

where $r(R,\epsilon,\alpha) = R(\sin^2\alpha + \epsilon^2\cos^2\alpha)^{1/2}$ and R is related to the radius of gyration through

$$R_g = \left(\frac{\epsilon^2 + 2\epsilon}{5}\right)^{1/2} R \tag{20}$$

Figure 11 shows the form factor curves calculated for a sphere ($\epsilon = 1$, curve a) and for ellipsoids with different degrees of ellipticity (up to $\epsilon = 4$, curve e). This range of ϵ covers the shapes of the simulated half-generation dendrimers, as inferred from their moments of inertia. Comparing with the $P(q)$ curves of generations 0.5 and 1.5 (Figure 10), it is evident that this model (of a homogeneous ellipsoid of revolution) fails to give an adequate description of the results for low generations. Prosa et al.[22] employ a soft-sphere or star-like polymer model to fit the SAXS scattering curves of low (integer) generation PAMAMs in methanol. Such model should, in principle, provide a better description of the sparse character of low generations, but the difficulty in obtaining proper fits prompts these authors to conclude that "excluded-volume effects and non-Gaussian statistics" must play a role "even for the smaller generation dendrimers". On the other hand, with increasing generation these dendrimers should develop the characteristics (in terms of spatial density distribution) amenable for modeling with geometrical models. Already for generation 2.5, we find that the $P(q)$ curve of configuration F (open circles in Figure 12A) compares well

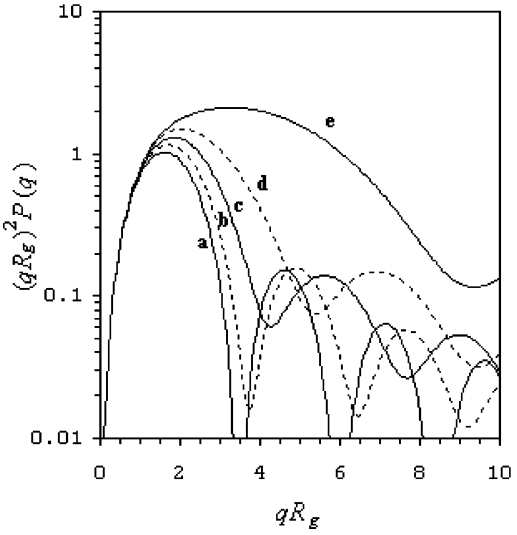

Figure 11. Form factor curves calculated from the model of a homogeneous ellipsoid of revolution using expression 19 for different degrees of ellipticity: (a) $\epsilon = 1$ (sphere), (b) $\epsilon = 1.2$, (c) $\epsilon = 1.5$, (d) $\epsilon = 2$, and (e) $\epsilon = 4$ (dashed lines alternate with full lines for better clarity).

with the form factor of an ellipsoid with $\epsilon = 1.7$ (dashed curve in upper position in the same figure). A similar comparison is not possible for the $P(q)$ curve of configuration E (closed circles in Figure 12A), which shows a small shoulder embedded in the first peak (the dashed curve that accompanies the closed circles is the plain average between curves a and d in Figure 11, and no particular meaning is attributed to the agreement observed here).

The situation for generation 3.5 is somewhat more complex (open triangles in Figure 10). In opposition to the trend observed for the neighboring generations, the first peak of the $P(q)$ curve for generation 3.5 increases in size and the maximum shifts to higher qR_g values. Two models were considered here for comparison purposes: an ellipsoid of revolution with $\epsilon = 1.9$ (dashed curve in upper position in Figure 12B) and a Gaussian shell with radial symmetry (dot−dashed curve in the same figure). The latter model was suggested by the radial density distribution obtained for generation 3.5 in our simulations (Figure 6D), which shows a pronounced minimum at the center-of-mass, followed by a region of approximately constant density that smoothly smears out in the dendrimer's periphery. Therefore, a Gaussian function was fitted to the density distribution profile and the parameters retrieved were used to calculate the respective form factor. Both models show trends that qualitatively resemble those of the $P(q)$ curve for generation 3.5, and a full description could probably be attained with a model incorporating features from the two models (ellipticity and nonhomogeneous density profile).

Finally, the $P(q)$ curve of generation 4.5 (closed squares in Figure 12B) is compared with the form factor of a hard sphere (dashed curve in lower position in the same figure). The positions of the first maximum and minimum for a perfect spherical body should occur at qR_g values of, respectively, 1.61 and 3.48 in the Kratky representation. These features appear in the $P(q)$ curve of generation 4.5, in agreement with the picture (recurrently mentioned) of convergence of the dendrimer shape toward sphericity with increasing generation. Such agreement is, however, lost in the high qR_g region, indicating that some characteristics of high-generation dendrimers are not yet fully developed in generation 4.5.[124]

Prosa et al.[22] show that it is possible to fit the SAXS scattering curves of PAMAM generations 9 and 10 with a hard-sphere model allowing for a Gaussian distribution of sizes. These authors also emphasize that this model and the model of monodisperse ellipsoids of revolution (eq 19) are indiscernible and assume that variations of both size and shape of the dendrimers occur in real systems. Furthermore, Nisato et al.[51] raise the question of ergodicity in these systems not only in respect to computational simulations of dendrimers but also in the real physical systems. Taking into account our results, in particular, the results for generation 2.5 where two slightly different configurations in terms of size and shape were identified, we are in a position to concur with both points of view. The values of ϵ retrieved by Prosa et al. (from fitting their SAXS results with the ellipsoidal model) are 1.93, 1.86,

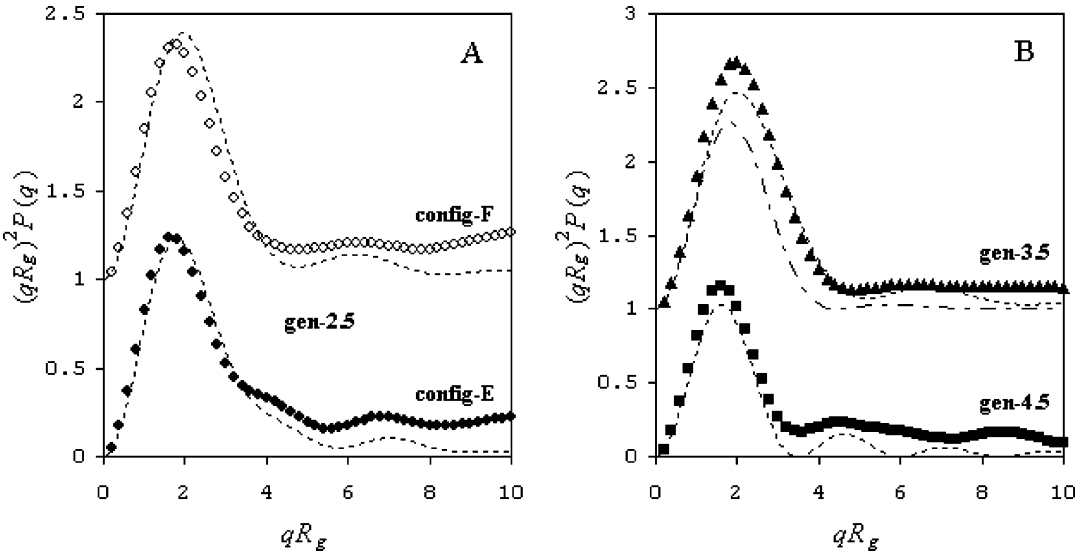

Figure 12. Comparison between the form factors calculated from the simulations and from simple models for selected generations: (A) generation 2.5, configuration F, open circles (shifted up by one unit), and configuration E, closed circles; (B) generation 3.5, closed triangle (shifted up by one unit), and generation 4.5, closed squares. Dashed curve in upper position in (A) is the form factor for an ellipsoid with $\epsilon = 1.7$ and dashed curve in lower position is the plain average between curves (a) and (d) in Figure 11; dashed curve in upper position in (B) is the form factor for an ellipsoid with $\epsilon = 1.9$, and the dot−dashed curve also in upper position is the form factor for a Gaussian shell model; dashed curve in lower position in (B) is the form factor for a perfect sphere.

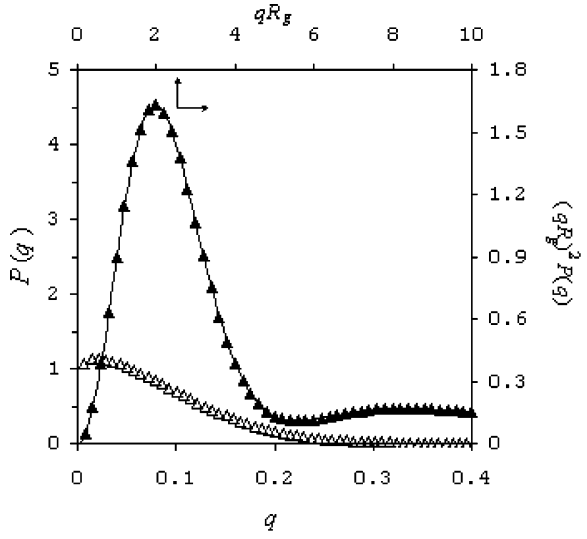

Figure 13. Form factor calculated for the simulation of generation 3.5 considering a permittivity constant of $\epsilon = 32.7$ (methanol) in direct representation (open triangles, left and lower axes) and in the Kratky representation (closed triangles, right and upper axes).

and 1.44 for generations 3, 4, and 5, respectively. These values are comparable to the average ratio of the principal moments of inertia obtained in our simulations for generations 2.5, 3.5, and 4.5, which are $\langle \overline{I_{y,z}}/I_x \rangle = 2.12$, 1.92, and 1.27, respectively (see Figure 5).[125]

It would be interesting to compare the form factors calculated from dendrimer simulations against results of SAXS or SANS for half-generation PAMAMs. However, to the best of our knowledge, we could only find one example in the literature of a study using SAXS technique to investigate the structure of PAMAM generations 2, 3.5, and 4 in methanol.[126,127] To this purpose, we performed a simulation of generation 3.5 considering a permittivity constant of $\epsilon = 32.7$ for the calculation of electrostatics (which corresponds to the permittivity of methanol at 298K) and a simulation box with a length of 172.1 Å (this is equivalent to a dendrimer concentration of 3.26×10^{-4} M). The simulation yielded a radius of gyration of 13.9 Å (practically identical to the R_g value obtained in the previous conditions; see Table 2). Using expression 20 with $\epsilon = 1$ (approximation to spherical shape), this value is converted to a particle diameter of 35.8 Å. Micali et al.[126] obtained good comparison between the experimental structure factor $S(q)$ of a dendrimer solution with concentration 3.26×10^{-3} M and a statistical-mechanical model for charged colloids using a particle diameter of 34 Å and an effective charge of $Z_{eff} = 6e$ for generation 3.5. We have used the Poisson−Boltzmann equation and Bjerrum criterion to estimate the effective charge (Section 3C) of the dendrimer in the same conditions and calculated a value of $Z_{eff} = 4.4e$. Furthermore, the radial distribution of counterions extracted from the simulation (not shown here) follows a trend close to the solution of Poisson−Boltzmann equation. The form factor calculated from the same simulation is shown in Figure 13 (open triangles), and it can be directly compared with the scattering intensity curve measured by Micali et al. for their lowest concentration of generation 3.5 (closed circles in Figure 2 of reference 126), in which case $S(q) \sim 1$. Unfortunately, the experimental data is not presented in the Kratky representation, which would facilitate comparison to the simulation results because the features of the form factor curve become more evident (see closed triangles in Figure 13 for the Kratky representation of the $P(q)$ curve shown in the same figure as open triangles). Nevertheless, taking into consideration the R_g, Z_{eff}, and $P(q)$ data obtained from our simulation, it is reasonable to state that general agreement is observed between experimental results and theoretical or simulation models.[128]

4. Conclusions

Atomistic molecular dynamics simulations were employed to study half-generation PAMAM dendrimers up to generation 4.5. The simulated dendrimers have negatively charged end-groups that are compensated by an equal number of sodium counterions. From the simulation results, several structural properties of these systems were evaluated like the size and shape of the dendrimers or the radial distributions of counterions. The average radius of gyration of generations 2.5 to 4.5 obeys the same scaling law $R_g \approx M^{1/d_f}$ that was verified in previous simulations of full-generation PAMAMs without explicit solvent. The value retrieved for the fractal dimension, $d_f \cong 3$, indicates that these are space-filling objects. The R_g values of generations 0.5 and 1.5 fall slightly above from that scaling law. It is qualitatively argued that electrostatic interactions must have a stronger influence in the conformation of low-generation dendrimers. In this case, the counterion concentrations are lower and the screening effects, which could dim the repulsion between the charged end-groups, are not so significant. This hypothesis is supported by calculations of the Debye screening length and from estimates of the dendrimer's effective charge using Poisson−Boltzmann cell model and Bjerrum criterion for the several generations simulated. In fact, charge renormalization due to counterion condensation is more pronounced with increasing generation. The radial distributions of counterions from the simulations are in close agreement with the solutions of Poisson−Boltzmann equation, which signifies that ion−ion correlation effects are negligible for the particle density in the simulated systems (i.e., the dendrimer concentration). The ratios of the principal moments of inertia indicate that the shape of the simulated dendrimers correspond approximately to a prolate ellipsoid. This information was used to compare the form factors extracted from the simulations with the model of a homogeneous ellipsoid of revolution. Even though full agreement was not attained with this simple geometrical model, some features of the form factor curves are fairly described for the generations above 2.5. In particular, the curve obtained for generation 4.5 is reasonably approximated by the form factor of a hard sphere in the lower qR_g region of the Kratky plot. This result is in conformity with previous atomistic simulations of PAMAM dendrimers that claim a morphological transition to a more compact and spherical conformation for generations above 3−4.[41,46,48] More experimental studies about the structural properties of half-generation PAMAMs are lacking. We have compared our simulation results with those of a study of generation 3.5 in methanol using the SAXS technique, and general agreement was found. However, the influence of solvent quality or pH and ionic strength in the size and shape of flexible-chain dendrimers is a subject that still allows for further studies from both the computational and experimental standpoints.

Acknowledgment. This work was financially supported by CQE IV under the project POCTI/QUI/35398/2000. P.M.R. Paulo acknowledges a Ph.D. grant BD 21698/99 from FCT under the program Praxis XXI. Partial financial support by the Fundação Calouste Gulbenkian is also gratefully acknowledged.

Supporting Information Available: Parameters of the force field employed in the dendrimer simulations. This material is available free of charge via the Internet at http://pubs.acs.org.

References and Notes

(1) Tomalia, D. A.; Baker, H.; Dewald, J.; Hall, M.; Kallos, G.; Martin, S.; Roeck, J.; Ryder, J.; Smith, P. *Polym. J.* **1985**, *17*, 117.

(2) Janssen, H. M.; Meijer, E. W. In *Synthesis of Polymers: Materials Science and Technology Series*; Schüter, A. D., Ed.; Cahn, R. W., Haasen, P., Kramer, E. J., series Eds.; Wiley−VCH: Weinheim, 1999; p 403.

(3) Fischer, M.; Vögtle, F. *Angew. Chem., Int. Ed.* **1999**, *38*, 884−905.

(4) Zeng, F.; Zimmerman, S. C. *Chem. Rev.* **1997**, *97*, 1681.

(5) Matthews, O. A.; Shipway, A. N.; Stoddart, J. F. *Prog. Polym. Sci.* **1998**, *23*, 1.

(6) Tomalia, D. A.; Naylor, A. M.; Goddard, W. A., III. *Angew. Chem., Int. Ed. Engl.* **1990**, *29*, 138.

(7) Tomalia, D. A.; Huang, B.; Swanson, D. R.; Brothers, H. M., II; Klimash, J. W. *Tetrahedron* **2003**, *59*, 3799.

(8) Chow, H.-F.; Mong, T. K.-K.; Chan, Y.-H.; Cheng, C. H. *Tetrahedron* **2003**, *59*, 3915.

(9) Diederich, F.; Felber, B. *Proc. Natl. Acad. Sci. U.S.A.* **2002**, *99*, 4779.

(10) Liu, L.; Breslow, R. *J. Am. Chem. Soc.* **2003**, *125*, 12110.

(11) Vögtle, F.; Gestermann, S.; Hesse, R.; Schwierz, H.; Windisch, B. *Prog. Polym. Sci.* **2000**, *25*, 987.

(12) Adronov, A.; Fréchet, J. M. J. *Chem. Commun.* **2000**, *18*, 1701.

(13) Freeman, A. W.; Koene, S. C.; Malenfant, P. R. L.; Thompson, M. E.; Fréchet, J. M. J. *J. Am. Chem. Soc.* **2000**, *122*, 12385.

(14) Balzani, V.; Ceroni, P.; Gestermann, S.; Kauffmann, C.; Gorkab, M.; Vögtle, F. *Chem. Commun.* **2000**, *10*, 853.

(15) Fréchet, J. M. J. *Proc. Natl. Acad. Sci. U.S.A.* **2002**, *99*, 4782.

(16) Zimmerman, S. C.; Zeng, F.; Reichert, D. E. C.; Kolotuchin, S. V., *Science* **1996**, *271*, 1095.

(17) Jansen, J. F. G. A.; de Brabander-van den Berg, E. M. M.; Meijer, E. W. *Science* **1994**, *266*, 1226.

(18) Jockush, S.; Ramirez, J.; Sanghvi, K.; Nociti, R.; Turro, N. J.; Tomalia, D. A. *Macromolecules* **1999**, *32*, 4419.

(19) Ottaviani, M. F.; Montalti, F.; Romanelli, M.; Turro, N. J.; Tomalia, D. A. *J. Phys. Chem.* **1996**, *100*, 11033.

(20) Stechemesser, S.; Eimer, W. *Macromolecules* **1997**, *30*, 2204.

(21) Prosa, T. J.; Bauer, B. J.; Amis, E. J.; Tomalia, D. A.; Scherrenberg, R. *J. Polym. Sci., Part B: Polym. Phys.* **1997**, *35*, 2913.

(22) Prosa, T. J.; Bauer, B. J.; Amis, E. J. *Macromolecules* **2001**, *34*, 4897.

(23) Mallmace, F.; Canetta, E.; Lombardo, D.; Mazzaglia, A.; Romeo, A.; Monsù, Scolaro, L.; Maino, G. *Physica A* **2002**, *304*, 235.

(24) Rathgeber, S.; Monkenbusch, M.; Kreitschmann, M.; Urban, V.; Brulet, A. *J. Chem. Phys.* **2002**, *117*, 4047.

(25) Meltzer, A. D.; Tirrel, D. A.; Jones, A. A.; Inglefield, P. T.; Hedstrand, D. M.; Tomalia, D. A. *Macromolecules* **1992**, *25*, 4541.

(26) Meltzer, A. D.; Tirrel, D. A.; Jones, A. A.; Inglefield, P. T. *Macromolecules* **1992**, *25*, 4549.

(27) Li, J.; Piehler, L. T.; Qin, D.; Baker, J. R., Jr.; Tomalia, D. A. *Langmuir* **2000**, *16*, 5613.

(28) Jackson, C. L.; Chanzy, H. D.; Booy, F. P.; Drake, B. J.; Tomalia, D. A.; Bauer, B. J.; Amis, E. J. *Macromolecules* **1998**, *31*, 6259.

(29) Cai, C.; Chen, Z. Y. *Macromolecules* **1998**, *31*, 6393.

(30) Cakara, D.; Kleimann, J.; Borkovec, M. *Macromolecules* **2003**, *36*, 4201.

(31) Niu, Y.; Sun, L.; Crooks, R. M. *Macromolecules* **2003**, *36*, 5725.

(32) Ottaviani, M. F.; Bossmann, S.; Turro, N. J.; Tomalia, D. A. *J. Am. Chem. Soc.* **1994**, *116*, 661.

(33) Ottaviani, M. F.; Montalti, F.; Turro, N. J.; Tomalia, D. A. *J. Phys. Chem. B* **1997**, *101*, 158.

(34) de Gennes, P. G.; Hervet, H. J. *J. Phys. (Paris*) **1983**, *44*, L351.

(35) Boris, D.; Rubinstein, M. *Macromolecules* **1996**, *29*, 7251.

(36) von Ferber, C.; Blumen, A. *J. Chem. Phys.* **2002**, *117*, 8616.

(37) Timoshenko, E. G.; Kuznetsov, Y. A.; Connolly, R. *J. Chem. Phys.* **2002**, *117*, 9050.

(38) Wolterink, J. K.; van Male, J.; Daoud, M.; Borisov, O. V. *Macromolecules* **2003**, *36*, 6624.

(39) Borkovec, M.; Koper, G. J. M. *Macromolecules* **1997**, *30*, 2151.

(40) Sun, L.; Crooks, R. M. *J. Phys. Chem. B* **2002**, *106*, 5864.

(41) Naylor, A. M.; Goddard, W. A., III; Kiefer, G. E.; Tomalia, D. A. *J. Am. Chem. Soc.* **1989**, *111*, 2339.

(42) Lescanec, R. L.; Muthukumar, M. *Macromolecules* **1990**, *23*, 2280.

(43) Mansfield, M. L.; Klushin, L. I. *Macromolecules* **1993**, *26*, 4262.

(44) Murat, M.; Grest, G. S. *Macromolecules* **1996**, *29*, 1278.

(45) Lyulin, A. V.; Davies, G. R.; Adolf, D. B. *Macromolecules* **2000**, *33*, 6899.

(46) Lee, I.; Athey, B. D.; Wetzel, A. W.; Meixner, W.; Baker, J. R., Jr. *Macromolecules* **2002**, *35*, 4510.

(47) Terao, T.; Nakayama, T. *Macromolecules* **2004**, *37*, 4686.

(48) Maiti, P. K.; Çağin, T.; Wang, G.; Goddard, W. A., III. *Macromolecules* **2004**, *37*, 6236.

(49) Nisato, G.; Ivkov, R.; Amis, E. J., *Macromolecules* **1999**, *32*, 5895.

(50) Topp, A.; Bauer, B. J.; Tomalia, D. A.; Amis, E. J. *Macromolecules* **1999**, *32*, 7232.

(51) Nisato, G.; Ivkov, R.; Amis, E. J., *Macromolecules* **2000**, *33*, 4172.

(52) Welch, P.; Muthukumar, M. *Macromolecules* **1998**, *31*, 5892.

(53) Maiti, P. K.; Çağin, T.; Lin, S.-T.; Goddard, W. A., III. *Macromolecules* **2005**, *38*, 979.

(54) Maiti, P. K.; Goddard, W. A., III. *J. Phys. Chem. B* **2006**, *110*, 25628.

(55) Gurtovenko, A. A.; Lyulin, S. V.; Karttunen, M.; Vattulainen, I. *J. Chem. Phys.* **2006**, *124*, 094904.

(56) Maxwell, B. D.; Fujiwara, H.; Habibi-Goudarzi, S.; Ortiz, J. P.; Logusch, S. J. *J. Labelled Compd Radiopharm.* **1998**, *41*, 935.

(57) Malik, N.; Wiwattanapatapee, R.; Klopsch, R.; Lorenz, K.; Frey, H.; Weener, J. W.; Meijer, E. W.; Paulus, W.; Duncan, R. *J. Controlled Release* **2000**, *65*, 133.

(58) Wiwattanapatapee, R.; Carreño-Gómez, B.; Malik, N.; Duncan, R. *Pharm. Res.* **2000**, *17*, 991.

(59) Khopade, A. J.; Khopade, S.; Jain, N. K. *Int. J. Pharm.* **2002**, *241*, 145.

(60) Jevprasesphant, R.; Penny, J.; Attwood, J.; McKeown, N. B.; D'Emanuele, A. *Pharm. Res.* **2003**, *20*, 1543.

(61) Devarakonda, B.; Hill, R. A.; Liebenberg, W.; Brits, M.; de Villiers, M. M. *Int. J. Pharm.* **2005**, *304*, 193.

(62) Vandamme, Th. F.; Brobeck, L. *J. Controlled Release* **2005**, *102*, 23.

(63) Yang, H.; Lopina, S. T. *J. Biomed. Mater. Res.* **2005**, *72A*, 107.

(64) Shcharbin, D.; Bryszewska, M. *Biochim. Biophys. Acta* **2006**, *1760*, 1021.

(65) Howell, B. A.; Fan, D.; Rakesh, L. *J. Therm. Anal. Calorim.* **2006**, *85*, 17.

(66) Gurdag, S.; Khandare, J.; Stapels, S.; Matherly, L. H.; Kannan, R. M. *Bioconjugate Chem.* **2006**, *17*, 275.

(67) Naka, K.; Tanaka, Y.; Chujo, Y.; Ito, Y. *Chem. Commun.* **1999**, 1931.

(68) Tanaka, Y.; Nemoto, T.; Naka, K.; Chujo, Y. *Polym. Bull.* **2000**, *45*, 447.

(69) Cooper, S. J. *Cryst. Eng. Commun.* **2001**, *56*, 1.

(70) Naka, K.; Tanaka, Y.; Chujo, Y. *Langmuir* **2002**, *18*, 3655.

(71) Naka, K.; Chujo, Y. *C. R. Chimie* **2003**, *6*, 1193.

(72) Zhang, F.; Yang, S.-P.; Chen, H.-M.; Wang, Z.-H.; Yu, X.-B. *J. Cryst. Growth* **2004**, *267*, 569.

(73) Zhang, F.; Yang, S.-P.; Wang, W.-M.; Chen, H.-M.; Wang, Z.-H.; Yu, X.-B. *Mater. Lett.* **2004**, *58*, 3285.

(74) Zhang, F.; Zhou, Z.-H.; Yang, S.-P.; Mao, L.-H.; Chen, H.-M.; Yu, X.-B. *Mater. Lett.* **2005**, *59*, 1422.

(75) Volden, S.; Glomm, W. R.; Magnusson, H.; Øye, G.; Sjöblom, J. *J. Dispersion Sci. Technol.* **2006**, *27*, 893.

(76) Xu, Y.; Dongye, Z. *Environ. Sci. Technol.* **2005**, *39*, 2369.

(77) Islam, M. T.; Shi, X.; Balogh, L.; Bajer, Jr., J. R. *Anal. Chem.* **2005**, *77*, 2063.

(78) He, M.; Emory, J. F.; McLuckey, S. A. *Anal. Chem.* **2005**, *77*, 3173.

(79) Ottaviani, M. F.; Turro, N. J.; Jockush, S.; Tomalia, D. A. *Colloids Surf. A* **1996**, *115*, 9.

(80) Bakshi, M. S.; Kaura, A. *Colloids Surf. A* **2004**, *244*, 45.

(81) Bakshi, M. S.; Kaura, A.; Mahajan, R. K.; Yoshimura, T.; Esumi, K. *Colloids Surf. A* **2004**, *246*, 39.

(82) Bakshi, M. S.; Sood, R.; Gurvinder, K.; Ranganathan, R. *Colloid. Polym. Sci.* **2005**, *284*, 233.

(83) Wang, J.; Chen, J.; Jia, X.; Cao, W.; Li, M. *Chem. Commun.* **2000**, 511.

(84) Lin, W.; Galletto, P.; Borkovec, M. *Langmuir* **2004**, *20*, 7465.

(85) Wade, D. A.; Torres, P. A.; Tucker, S. A. *Anal. Chim. Acta* **1999**, *397*, 17.

(86) Larson, C. L.; Tucker, S. A. *Appl. Spectrosc.* **2001**, *55*, 679.

(87) Wade, D. A.; Mao, C.; Hollenbeck, A. C.; Tucker, S. A. *Fresenius J. Anal. Chem.* **2001**, *369*, 378.

(88) Shcharbin, D.; Klajnert, B.; Mazhul, V.; Bryszewska, M. *J. Fluoresc.* **2005**, *15*, 21.

(89) Paulo, P. M. R.; Costa, S. M. B. *J. Phys. Chem. B* **2005**, *109*, 13928.

(90) Jorgensen, W. L.; Tirado-Rives, J. *J. Am. Chem. Soc.* **1988**, *110*, 1657.

(91) Pranata, J.; Wierschke, S. G.; Jorgensen, W. L. *J. Am. Chem. Soc.* **1991**, *113*, 2810.

(92) Jorgensen, W. L.; McDonald, N. A. *J. Mol. Struct. (THEOCHEM*) **1998**, *424*, 145.

(93) Mahoney, M. W.; Jorgensen, W. L. *J. Chem. Phys.* **2000**, *112*, 8910.

(94) Jorgensen, W. L.; Maxwell, D. S.; Tirado-Rives, J. *J. Am. Chem. Soc.* **1996**, *118*, 11225.

(95) Kaminski, G. A.; Jorgensen, W. L. *J. Phys. Chem.* **1996**, *100*, 18010.

(96) Kaminski, G. A.; Friesner, R. A.; Tirado-Rives, J.; Jorgensen, W. L. *J. Phys. Chem. B* **2001**, *105*, 6474.

(97) Rizzo, R. C.; Jorgensen, W. L. *J. Am. Chem. Soc.* **1999**, *121*, 4827.
(98) McDonald, N. A.; Jorgensen, W. L. *J. Phys. Chem. B* **1998**, *102*, 8049.
(99) Weiner, S. J.; Kollman, P. A.; Case, D. A.; Singh, U. C.; Ghio, C.; Alagona, G.; Profeta, S., Jr.; Weiner, P. *J. Am. Chem. Soc.* **1984**, *106*, 765.
(100) Cornell, W. D.; Cieplak, P.; Bayly, C. I.; Gould, I. R.; Merz, K. M., Jr.; Ferguson, D. M.; Spellmeyer., D. C.; Fox, T.; Caldwell, J. W.; Kollman, P. A. *J. Am. Chem. Soc.* **1995**, *117*, 5179.
(101) Paulo, P. M. R.; Gronheid, R.; De Schryver, F. C.; Costa, S. M. B. *Macromolecules* **2003**, *36*, 9135.
(102) Forester, T. R.; Smith, W. In *The DL_POLY_2 Reference Manual* version 2.12; CCLRC: Daresbury Laboratory, 1999; http://www.cse.clrc.ac.uk/msi/software/DL_POLY/MANUALS/USRMAN2/USRMAN.html).
(103) Melchionna, S.; Ciccotti, G.; Holian, B. L. *Molec. Phys.* **1993**, *78*, 53.
(104) In the case of half-generations, this formula holds by rounding g to the next higher integer value.
(105) No particular relevance is attributed to the greater sphericity of generation 0.5 in relation to generation 1.5. This is probably related to the fact that the conformation of generation 0.5 is more conditioned by the tetrahedral symmetry of the dendrimer core.
(106) Rudnick, G.; Gaspari, G. *J. Phys. A* **1986**, *4*, L191.
(107) The first Heavyside function appearing in the right-hand side of expression 8 should be defined with $H(0) = 1$, while the second function should be defined with $H(0) = 0$.
(108) Belloni, L. *Colloids Surf. A* **1998**, *140*, 227.
(109) Belloni, L.; Drifford, M.; Turq, P. *Chem. Phys.* **1984**, *83*, 147.
(110) About the top limit of the integral in expression 9, it defines the length of the cell and is inversely related to the polyelectrolyte concentration.
(111) Notice, however, that the counterion radial distributions calculated from the simulations extend to radial distances below the dendrimer's hydrodynamic radius because these are not impenetrable spheres as assumed in the P−B cell model.
(112) Manning, G. S. *J. Chem. Phys.* **1969**, *51*, 924 and 934.
(113) Manning, G. S. *J. Chem. Phys.* **1969**, *51*, 3249.
(114) Huang, Q. R.; Dublin, P. L.; Moorefield, C. N.; Newkome, G. R. *J. Phys. Chem. B* **2000**, *104*, 898.
(115) The model dendrimer considered in ref 55 is a fourth-generation dendrimer with a trifunctional core and branching multiplicity 2. This topology corresponds to a total of 48 terminal groups. Because the PAMAM dendrimers simulated in this work have a tetrafunctional core, none of them matches the same stoichiometry of terminal groups (Table 1).
(116) The simulation box used in ref 55 has a length of $14.16l_0$, where l_0 is a reference bond length which assumes the suggested value of approximately 6.7 Å for PAMAM dendrimer. This gives a box length of 94.9 Å that is smaller than any of the simulations boxes used in the present work.
(117) Allen, M. P.; Tildesley, D. J. In *Computer Simulation of Liquids*; Claredon Press: Oxford, 1989.
(118) Becker, O. M.; Karplus, M. *J. Chem. Phys.* **1997**, *106*, 1495.
(119) The box length of 321.4 Å or, equivalently, the dendrimer concentration of 0.05 mM, correspond to the standard conditions used for the simulations reported in the other sections of this paper, as it is mentioned in Section 2.
(120) The estimates of Z_{eff} from the P−B model were calculated by considering a constant radius of 14.5 Å for generation 2.5 regardless of the dendrimer concentration, which is a first approximation, in view of the results shown in Section 3D.
(121) The integrals appearing in expression 16 were numerically evaluated using trapezoidal rule with a step of 9° for both polar and azimuthal coordinates. The final $P(q)$ curve resulted from averaging over 21 conformations equally spread during the last 100 ps of simulation.
(122) Experimentally, the quantity q is referred to as the scattering vector and is defined as $q = (4\pi/\lambda)\sin(\theta)$ where λ is the wavelength of the incident radiation and θ is the angle between the incident and scattered beams.
(123) Pedersen, J. S. *Adv. Colloid Interface Sci.* **1997**, *70*, 171.
(124) Early computational and experimental studies of full-generation PAMAMs with amine core showed that a morphological transition from an open and oblate dendrimer conformation to a more compact and spherical structure occurs around generation 3.[41] Recent computational studies (ref 46) of full-generation PAMAMs with ethylenediamine core (which is "larger" than the amine core) indicate, however, that this transition occurs one generation up, i.e., around generation 4. Our simulations involve ethylenediamine−core PAMAMs, and for that reason we refer to generations 3.5 and 4.5 as intermediate generations.
(125) Here $\overline{I_{y,z}}$ means the average over the moments of inertia I_y and I_z, and $\langle(\cdots)\rangle$ represents the average over the various configurations sampled from the simulations.
(126) Micali, N.; Monsu Scolaro, L.; Romeo, A.; Lombardo, D.; Lesieur, P.; Mallamace, F. *Phys. Rev. E* **1998**, *58*, 6229.
(127) The fact that the study of ref 126 involves both full- and half-generation PAMAMs allows for some comparison between them. In particular, it is shown that methanol solutions of half-generation PAMAM display an ordering effect due to long-range electrostatic interactions from partial ionization of the dendrimer's terminal carboxylate groups that are not present in the integer generations. On the other hand, Nisato et al. (ref 49) have proved through SANS technique that full-generation PAMAM in aqueous solution under appropriate pH and ionic strength conditions also display liquid-like ordering effects.
(128) Micali et al. (ref 126) derive an interesting conclusion from their data analysis, which is the absence of variation of the macroion charge number or Z_{eff} in the range of dendrimer concentration investigated by them. The same conclusion is not reached by us from our estimates using the Poisson−Boltzmann equation, which give a charge renormalization from $Z_{\text{eff}} = 8.1e$ down to $3.8e$ as the concentration of macroion is increased from 6.5×10^{-4} to 6.52×10^{-3} M.